Trapping of the OH Radical by α-Tocopherol: A Theoretical Study

M. Navarrete, C. Rangel, J. C. Corchado, and J. Espinosa-García*

Departamento de Química Física, Universidad de Extremadura, 06071 Badajoz, Spain

Received: February 9, 2005; In Final Form: April 7, 2005

The antioxidant activity of α-tocopherol against the damaging hydroxyl radical was analyzed theoretically by hybrid density functional theory, following the direct dynamics method, where the thermal rate constants were calculated using variational transition-state theory with multidimensional tunneling. We found that the OH radical is only slightly or not at all selective, attacking by different mechanisms at several positions of the α-tocopherol molecule, giving competitive reactions. The most favorable pathways are the hydrogen abstraction reaction from the phenolic hydrogen and the electrophilic addition onto the aromatic ring. We propose a final rate constant, the sum of the competitive hydrogen abstraction and addition reactions, $\geq 2.7 \times 10^8$ M^{-1} s^{-1} at 298 K, where the hydrogen abstraction reaction represents only 20% of the total OH radical reaction. This result indicates that, molecule by molecule, in an apolar environment, α-tocopherol is less effective than coenzyme Q (which presents a rate constant of 6.2×10^{10} M^{-1} s^{-1} at 298 K) as a scavenger of OH radicals. It was also found that both mechanisms are not direct but pass through intermediates in the entry channel, with little or no influence on the dynamics of the reactions. The hydrogen abstraction reaction also presents another intermediate in the exit channel, which may have a significant role in preventing the pro-oxidant effects of α-tocopherol, although less important than with free radicals other than OH.

1. Introduction

In recent years, the frontier between chemistry and biochemistry has become even more diffuse. Theoretical chemists are interested in larger molecular systems, such as enzyme or solvent effects, with biological implications. From a theoretical point of view, the study of large molecular systems using ab initio calculations with correlated wave functions is today still prohibitive, and the search for economic and adequate alternatives represents a challenge for theoretical chemists. Density functional theory (DFT) allows the calculation of the structures and properties of very large molecules with reasonable computational effort.

The role of natural antioxidants has lately received much attention because they can avoid or at least significantly reduce the peroxidation of lipids by free radicals, which is related to a variety of disorders and diseases.[1] α-Tocopherol (α-TOH), the most active form of vitamin E, and coenzyme Q (CoQ) partition in the lipid bilayer and are the most important lipid-soluble free radical trapping antioxidants. Experimentally, it has been found that the relative antioxidant activities of α-TOH versus CoQ are the following: CoQ > α-TOH in low-density lipoproteins (LDLs), CoQ < α-TOH in homogeneous solution, and CoQ ≈ α-TOH in aqueous lipid dispersion.[2]

However, α-TOH can also act as a pro-oxidant molecule[3] as a consequence of the relatively long life of the α-tocopheryl radical (α-TO•) formed after the hydrogen abstraction reaction

$$\alpha\text{-TOH} + \text{R}\bullet \rightarrow \alpha\text{-TO}\bullet + \text{RH}$$

takes place. Thus, this α-TO• radical can react with lipids present in the nearest environment, thereby increasing the lipid peroxidation. Fortunately, the rate of the hydrogen abstraction reaction from lipids is very slow.

Therefore, the study of the antioxidant activity is an exciting challenge for theoretical calculations, and given the experimental interest, our laboratory has performed a broad study of the activity of α-TOH and CoQ with the very damaging OH and OOH free radicals. Thus, in previous work, we studied for the first time the mechanism and kinetics of reactions between CoQ and the OH radical (theoretically and experimentally),[4] between CoQ and the OOH radical,[5] and between α-TOH and the OOH radical[6] (latter two only theoretically). For both antioxidants, it was found that the reactivity of the hydroperoxy radical is dominated by the hydrogen abstraction mechanism from the phenolic hydrogen with rate constants at 298 K of 5.3×10^5 and 1.5×10^5 M^{-1} s^{-1} for ubiquinol (reduced form of CoQ) and α-TOH, respectively. These rates agree with the experimental evidence in LDL, which lends confidence to the model and the method used in the theoretical study. In the case of the OH free radical, the reactivity is dominated by the addition mechanism on ubiquinone (oxidized form of CoQ), with a theoretical rate constant at 298 K of 2.1×10^{10} M^{-1} s^{-1} (experimental value 6.2×10^{10}), that is, practically diffusion-controlled.

To complete the study of the activity of the two antioxidants, in the present work, we study the reactivity of α-tocopherol with the hydroxyl radical. The aim is threefold: first, to propose a mechanism to account for the attack of the hydroxyl radical on α-TOH; second, to obtain theoretical kinetics information; and third, to compare the antioxidant activity of the two potent natural radical scavengers, α-TOH and CoQ. In section 2, we describe the theoretical method, computational details, and model used in the work; results and discussion are given in section 3; and conclusions are presented in section 4.

2. Methods and Computational Details

2.1. Modeling. As in previous work with these antioxidants,[4−6] given the large size of the molecular system and the great number of calculations to be performed in the reaction path constructions, the real biological reaction was modeled in the

10.1021/jp050717e CCC: $30.25
Published on Web 05/05/2005

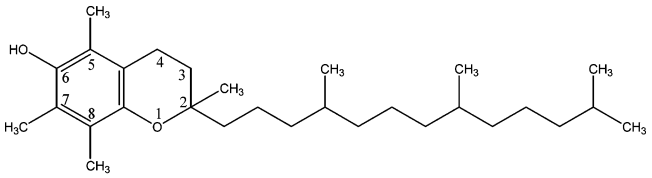

α-tocopherol

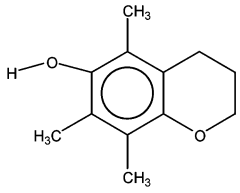

5, 7, 8-trimethyl-croman-6-ol

Figure 1. Numbering scheme for α-tocopherol and its model system employed in the present calculation.

following way. First, we replaced the trimethyltridecyl and methyl chains attached to carbon 2 in the α-tocopherol molecule by hydrogen atoms (see Figure 1). These chains have a prominent role in anchoring the α-tocopherol molecule to the membrane and restricting its mobility. However, it is very unlikely that they have any major influence on the reactivity of the system, since the reactive part of tocopherols is the cromanol ring, which has been kept unchanged in our model system. Moreover, these chains are protected by the lipidic environment against attack from cytosolic radicals, only part of the cromanol ring projects out from the membranes, and this is the only point where reactions with polar molecules solvated by cytosolic water can take place. We therefore modeled the α-tocopherol molecule by the 5,7,8-trimethyl-cromen-6-ol molecule (Figure 1). This same model and a similar model reducing the size of the real system had already been used with success in our previous studies of α-TOH[6] and CoQ,[4,5] respectively, and it is consistent with the conclusions of Foti et al.[7] that the hydrogen abstraction reaction from CoQ is independent of the size of the chain attached to the aromatic ring.

Second, while the theoretical study was performed in the gas phase, given the nonpolar character of the natural environment (lipid bilayer), one can reasonably assume that the conclusions will be roughly the same in the two environments. This same approximation had already been used with success in our previous experimental/theoretical study of CoQ with the OH radical.[4]

2.2. Electronic Structure Calculations. To handle these big size systems, an economic alternative involves density functional theory (DFT) methods. However, it is well-known that these methods generally underestimate the barrier height by several kilocalories per mole. For instance, Truhlar et al.[8a] performed an exhaustive study on a set of 22 reactions, finding that in general the DFT and hybrid DFT methods underestimate the barrier height by about 3.4 kcal mol^{-1}. Note that, for this same set of 22 reactions, the MP2 (second-order Möller−Plesset perturbation theory) ab initio level has a mean error of 5.8 kcal mol^{-1}, and the more expensive QCISD (quadratic configuration interaction with single and double excitations) ab initio level has a mean error of 3.5 kcal mol^{-1}, indicating the necessity to use highly correlated wave functions and large basis sets. With respect to the hybrid DFT methods, it has been found that the BHandHLYP method gives more accurate barrier heights than other hybrid DFT methods, such as B3LYP and B3P86,[8−11] and similar to the MPW1K DFT method of Truhlar et al.,[8a] and the development of new hybrid DFT methods is an area in continuous growth.[8b]

Geometries, energies, and first and second energy derivatives of all stationary points were calculated using hybrid density functional theory (DFT) as implemented in the Gaussian 98[12] suite of programs. Exchange and correlation were treated by the BHandHLYP method, which is based on Becke's half-and-half method[13] and the gradient-corrected correlation functional of Lee, Yang, and Parr,[14] using the 6-31G basis set.[15] We will denote this level by its usual abbreviation: BHandHLYP/6-31G (hereafter called Level 0).

Vibrational frequencies were calculated using Level 0 in order to check that these geometries correspond either to true minima on the potential energy surface, with all the vibrational frequencies being real, or to true saddle points, with a single imaginary frequency.

As was noted in the Introduction, the third aim of this work is the comparison of the antioxidant activity of CoQ and α-TOH, which obviously must be performed at the same level. Thus, as the first studies of this series with CoQ[4,5] were performed at the BHandHLYP/6-31G level, we use it also in the present work.

To check the accuracy of our calculations, we performed selected single-point calculations using both BHandHLYP and MPW1K functionals and larger basis sets, namely, 6-311G-(2d,p),[16] 6-311+G(d,p),[16] and 6-311++G(2d,2p).[16] These single-point calculations will be denoted by the usual double-slash notation: MPW1K/6-311G(2d,p)//Level 0 (hereafter called Level 1), BHandHLYP/6-311+G(d,p)//Level 0 (hereafter called Level 2), and BHandHLYP/6-311++G(2d,2p)//Level 0 (hereafter called Level 3).

2.3. Dynamics Calculations. Using Level 0, the "intrinsic reaction coordinate" (IRC), or minimum energy path (MEP), is constructed starting from the saddle-point geometry and going downhill to both the asymptotic reactant and product channels in mass-weighted Cartesian coordinates,[17] using Euler's integrator method with a step size of 0.05 b. The Hessian matrix is evaluated at every point along the reaction path, always avoiding the undesirable reorientations of molecular geometries. Along each MEP, the reaction coordinate, s, is defined as the signed distance from the saddle point, with $s > 0$ referring to the product side. We calculate the reaction path between $s = -1.5$ b and $s = +1.0$ b for the abstraction reaction and between $s = -5.0$ b and $s = +5.0$ b for the addition reaction.

Along each MEP, a generalized normal-mode analysis is performed projecting out frequencies at each point along the path using redundant internal coordinates.[18] With this information, the respective ground-state vibrationally adiabatic potential curve is calculated

$$V_a^G(s) = V_{MEP}(s) + \epsilon_{int}^G(s)$$

where $V_{MEP}(s)$ is the classical energy along each MEP with its zero energy at the reactants ($s = -\infty$) and $\epsilon_{int}^G(s)$ is the zero-point energy at s from the generalized normal-mode vibrations orthogonal to the reaction coordinate. The redundant coordinates chosen were all the possible bond lengths and angles. The advantage of redundant coordinates over rectilinear ones is that in some cases the lowest bending frequencies have unphysical imaginary values over a wide range of the reaction coordinate using rectilinear coordinates, whereas these frequencies are real over the whole reaction path using redundant coordinates.

With this previous information (energies, vibrational frequencies, geometries, and gradients along the MEP), the kinetics study of the selected reaction mechanisms of α-tocopherol with the hydroxyl radical was carried out using the direct dynamics approach[19] and a mapping interpolation procedure,[20] to minimize the errors caused by the limited information we calculated. Rate

constants were estimated using canonical variational transition-state theory (CVT),[21] which locates the dividing surface between reactants and products at a point $s^{*CVT}(T)$ along the reaction path that minimizes the generalized TST rate constants $k^{GT}(T,s)$ for a given temperature T. Thermodynamically, this is equivalent to locating the transition state at the maximum $\Delta G^{GT,\circ}[T,s^{*CVT}(T)]$ of the free energy of activation profile $\Delta G(T,s)$.[21] Thus, the thermal rate constant will be given by

$$k^{CVT}(T) = \sigma \frac{k_B T}{h} K^\circ \exp[-\Delta G(T,s^{*,CVT})/k_B T]$$

with k_B being Boltzmann's constant, h Planck's constant, σ the symmetry factor (the number of equivalent reaction paths, which were assumed to be 1 for the most favorable pathways, Rabs2 and Radd2), and K° the reciprocal of the standard-state concentration, taken as 1 molecule/cm^3.

In the present work, we correctly included the $^2\Pi_{1/2}$ excited state of OH (with an excitation energy of 140 cm^{-1}) in the reactant electronic partition function, and the rotational partition functions were calculated classically. Quantum effects on motions transversal to the reaction path were included using quantum-mechanical vibrational partition functions in the harmonic oscillator approach, while quantum effects on the motion along the reaction path were included using a semiclassical multidimensional method for tunneling, namely, the small-curvature tunneling method (SCT).[21] Kinetics calculations were performed using the Polyrate[22] and Gaussrate[23] computer codes.

To improve the description of the reaction paths, we calculated single-point energies at Levels 1−3 at the most relevant stationary points (reactants, products, wells, and saddle points). This information was conveniently interpolated using the VTST-ISPE (variational transition-state theory with interpolated single-point energies)[24] approach in order to perform dual-level kinetics calculations.[25] These dual-level kinetics calculations will be denoted using the recommended triple-slash notation, *X*//*Y*///*Z*, where the term to the right of the triple slash, *Z*, denotes the lower level (Level 0), while the term to its left, *X*//*Y*, denotes the higher level (Levels 1−3).

3. Results and Discussion

3.1. Possible Pathways of Attack. To study all the possible side reactions that can take place between α-tocopherol and the hydroxyl radical, we took two mechanisms into account: the hydrogen abstraction reaction and the reaction of addition to the aromatic ring. With respect to the hydrogen abstraction mechanism, we considered that the hydroxyl radical can abstract either the phenolic hydrogen (attached to the oxygen on carbon 6) or any of the methylic hydrogens (from the methyl groups attached to carbon atoms 5, 7, and 8). With respect to the addition reaction, we also take into account four addition centers, namely, carbons 5, 6, 7, and 8. Therefore, we took eight possible reactions into account, four hydrogen abstraction reactions and four addition reactions, as shown in Figure 2. Tables listing the geometries, energies, and vibrational frequencies of all stationary points are provided as Supporting Information.

The relative energies with respect to the reactants (reaction energy and barrier height) are listed in Table 1 at the BHandHLYP/6-31G level for the eight reactions. All reactions, both abstraction and addition, are very exothermic with low barrier heights, indicating that the attack of the OH radical on α-TOH is not very selective. Clearly, in the abstraction reaction, the difference in exothermicity between Rabs2 and the other reactions (Rabs1, Rabs3, and Rabs4) is due to the bond dissociation energies (BDEs) of the C−H bonds being usually higher than those of phenolic O−H bonds. For instance, the C−H bond dissociation energy in toluene is 88.5 kcal/mol[26] but the O−H bond dissociation energy for α-TOH is 77.3 kcal/mol.[27] This most exothermic reaction presents the lowest barrier height, and therefore, it will be the favorable abstraction reaction.

All four addition reactions are exothermic with very low barriers. This is the typical behavior for the electrophilic OH addition on the aromatic ring. The difference in barrier height between Radd4 and the other reactions (Radd1, Radd2, and Radd3) is due to the existence of a hydrogen bond between the

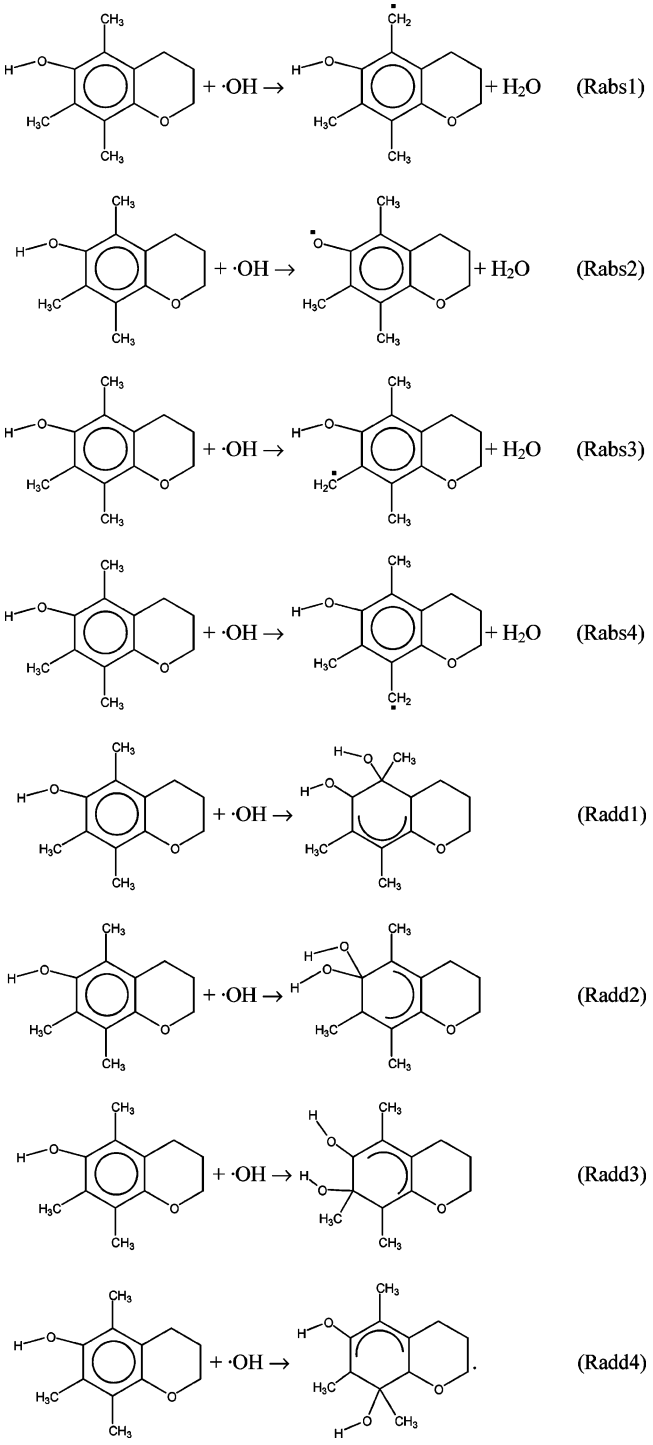

Figure 2. Reaction mechanisms taken into account for the α-tocopherol + •OH reaction.

TABLE 1: Relative Reaction Energies (kcal/mol) for the Eight Reactions and Selected Saddle Points at Level 0

approach	ΔE_R	$\Delta E^{\ddagger}$
Hydrogen Abstraction		
Rabs1	−14.3	+3.9
Rabs2	−29.6	−2.3
Rabs3	−13.5	+0.1
Rabs4	−14.0	+4.6
Addition		
Radd1	−10.9	−2.3
Radd2	−16.2	−3.8
Radd3	−16.5	−1.9
Radd4	−15.3	+2.6

OH attacking and the phenolic OH for the Radd1, Radd2, and Radd3 reactions, which is not possible for the Radd4 reaction. The Radd2 reaction presents the lowest barrier, and therefore, a priori, it will be the favorable addition reaction, although doubtless in view of the exothermicity and the low barrier of the other addition reactions, these will also contribute to the final rate constant.

One of the major aims of this paper is to propose a mechanism to account for the attack of the OH on α-TOH, that is, hydrogen abstraction or electrophilic addition. Therefore, due to the large size of the molecular system and the great number of calculations along the respective reaction paths, in the rest of the paper, we shall focus on the two most favorable pathways: the hydrogen abstraction reaction from the phenolic O−H, Rabs2, for the first case, and the addition reaction on atom 6, Radd2, for the second case. These results indicate that the OH radical is not very selective, and the abstraction and addition reactions are competitive (we shall return to this point later).

3.2. Hydrogen Abstraction Reaction, Rabs2. In this case, the attack of the hydroxyl radical on the phenolic O−H bond of the α-TOH proceeds via a weakly reactant hydrogen bonded complex (denoted HBR), a saddle point (SP), a product hydrogen bonded complex (denoted HBP), and the products (α-tocopheryl radical and water)

$$\alpha\text{-TOH} + \text{OH} \rightarrow \text{HBR} \rightarrow \text{SP} \rightarrow \text{HBP} \rightarrow \alpha\text{-TO}\bullet + \text{H}_2\text{O}$$

The optimized geometries at Level 0 are shown in Figure 3. It is interesting to observe the changes of some geometrical features as the reaction proceeds. The first stationary point from the reactants is a hydrogen bonded complex (HBR) close to the reactants, with a bond distance ($O\cdots H_1$) of 1.976 Å at this level. The other bond lengths and bond angles are close to those of the separated reactants.

Subsequently, a shortening of the $O\cdots H_1$ interatomic distance led us to a second stationary point, which was identified as having one imaginary frequency (1405 i cm^{-1}); that is, it is a true saddle point. The length of the bond that is broken increases by only 6%, while the length of the bond that is formed increases by 47% with respect to the reactant (α-TOH) and product (H_2O) molecules, respectively. Therefore, the reaction proceeds via an "early" transition state. This is the expected behavior that would follow from Hammond's postulate,[28] because the reaction is exothermic (see Figure 3).

Finally, another hydrogen bonded intermediate, denoted HBP, appears before the products and shows that the hydrogen of the H_2O product is bonded to the oxygen of the α-tocopheryl radical, with a distance of 1.836 Å. Along the reaction path, from reactants and products, the bond between carbon 6 and the phenolic oxygen is shortened. This is because the radical being formed is starting to take on part of the aromatic structure and the C−O bond is starting to take on some double-bond character.

3.2.1. Relative Energies. Figure 3 also plots the energy and enthalpy changes (0 and 298 K) of reaction and activation (estimated at the saddle point) for the Rabs2 reaction at Level 0. We shall begin by analyzing the reaction enthalpy. The experimental value of the reaction enthalpy at 298 K is −40.6 ± 1.0 kcal/mol, as predicted by the difference in bond dissociation energies of the O−H bond in α-tocopherol (77.3 ±1.0 kcal/mol)[27] and water (117.9 kcal/mol).[29] Thus, Level 0 predicts a reaction less exothermic than the experimental value. It is well-known that a major source of errors in standard theoretical calculations of molecular energies arises from truncation of the one-electron basis set. Hence, to study the influence of the level of calculation on the energy description of this reaction, we performed single-point calculations of the reaction energies, wells, and barrier height using different levels (Table 2). Levels 1−3 clearly improved the energy description of this reaction, with values of −35.8, −36.2, and −36.7 kcal/mol, respectively, close to the experimental result taking the error bar into account. In summary, Level 3 predicts the most exothermic reaction, and based on its best agreement with the only experimental magnitude available, the enthalpy of reaction at 298 K, it will be the level of calculation used in the remainder of the paper.

With respect to the barrier height, direct comparison with experiment or theoretical works is unfortunately not possible because no such information is available. We found that for the BHandHLYP functional when the level of calculation increases, the barrier height is higher, passing from a negative value (−2.3 kcal/mol) at Level 0 to a positive value (+0.8 kcal/mol) at Level 3. The MPW1K functional, however, does not improve the Level 0 description.

We shall analyze now the intermediate complexes. We have to note that the reactant complex is weakly bound, and its stability decreases as we increase the calculation level. This can be taken as an indication of the artificial stability afforded by the larger basis set superposition error of Level 0. Moreover, when we include the thermal effects, its enthalpy stability is reduced to 0.8, 1.4, and 1.1 kcal/mol at Levels 1−3, respectively, with respect to the reactants. Therefore, we can expect this well to have little influence on the mechanism of the reaction. However, the product complex, HBP, is significantly more stable than the products. When the thermal effects are included, this complex is even stabilized by 5.5, 5.1, and 3.6 kcal/mol at Levels 1−3, respectively, with respect to the products. It might therefore have some effect on the mechanism of the reaction. These results agree with those obtained for the reactions of the OOH radical with CoQ[5,30] and α-TOH,[6] where the hydrogen abstraction reaction is the dominant mechanism.

This high stability of the product well may suggest that in the exit channel the H_2O remains bonded to the α-tocopheryl radical for a certain time. This is a positive effect for the cell, avoiding or at least reducing its further attack on lipids in the membrane where it is anchored. In summary, in the study of two damaging free radicals, OH (present work) and OOH (ref 6), we have found that this effect decreases the pro-oxidant action of the newly formed α-tocopheryl radical. In the case of CoQ, to the best of our knowledge, this pro-oxidant effect has not been reported in the literature, neither experimentally nor theoretically. The existence of a very stabilized product well, −13.4 kcal/mol, for the CoQ + OOH hydrogen abstraction reaction would explain this behavior.

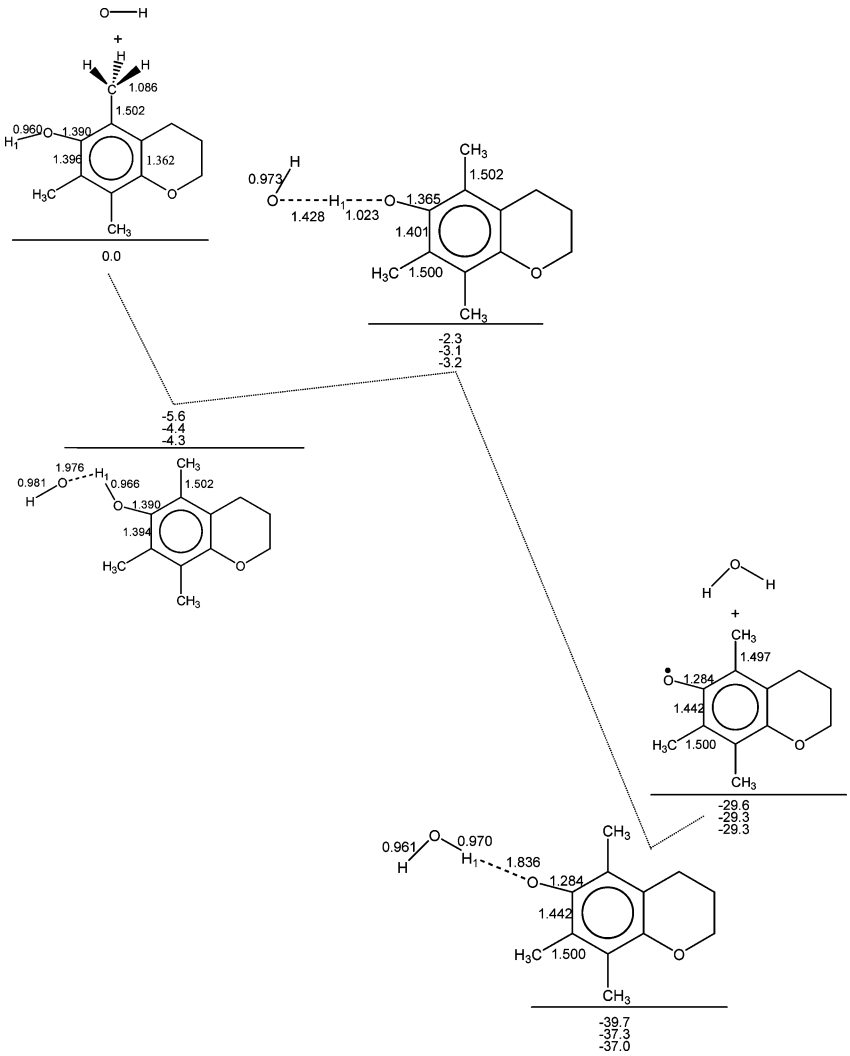

Figure 3. Reaction and barrier height energy (first entry) and enthalpy at 0 K (second entry) and 298 K (third entry) and geometric (bond lengths in angstroms) reaction profile of the OH + α-tocopherol hydrogen abstraction reaction, Rabs2, computed at the BHandHLYP/6-31G level of theory.

TABLE 2: Energy (Δ*E*) and Enthalpy (Δ*H*) at 298 K of Reaction (R), Activation (≠), and Wells for Rabs2 and Radd2 Reactions Using Different Levels of Calculation (kcal/mol)

	ΔE_R[a]	ΔH_R	$\Delta E^{\ddagger}$ [a]	$\Delta H^{\ddagger}$	ΔE_{HBR}[a,b]	ΔH_{HBR}	ΔE_{HBP}[c]	ΔH_{HBP}
				Rabs2 Abstraction Reaction				
Level 0[d]	−29.6	−29.3	−2.3	−3.2	−5.6	−4.4	−10.1	−7.7
Level 1[e]	−36.1	−35.8	−2.3	−3.2	−2.0	−0.8	−7.9	−5.5
Level 2[f]	−36.5	−36.2	+0.5	−0.4	−2.6	−1.4	−7.5	−5.1
Level 3[g]	−37.0	−36.7	+0.8	−0.1	−2.3	−1.1	−6.0	−3.6
exptl[h]		-40.6 ± 1.0						
				Radd2 Addition Reaction				
Level 0	−16.2	−13.4	−3.8	−2.4	−6.1	−4.3		
Level 1	−25.9	−23.1	−5.5	−4.1	−5.6	−3.8		
Level 2	−20.9	−18.1	−3.1	−1.7	−4.3	−2.5		
Level 3	−20.6	−17.8	−2.4	−1.0	−3.7	−1.9		

[a] With respect to the reactants. [b] Hydrogen bonded complex (HBR) for the Rabs2 reaciton and van der Waals complex (vdW) for the Radd2 reaction (see text). [c] With respect to the products. [d] Level 0: BHandHLYP/6-31G. [e] Level 1: MPW1K/6-311G(2d,p), single-point calculation. [f] Level 2: BHandHLYP/6-311+G(d,p), single-point calculation. [g] Level 3: BHandHLYP/6-311++G(2d,2p), single-point calculation. [h] From differences of BDEs (O−H) (see text).

3.3. Addition Reaction, Radd2. The attack of the electrophilic OH on the aromatic ring proceeds via a van der Waals complex (vdW), a saddle point (SP), and the adduct product

$$\alpha\text{-TOH} + \text{OH} \rightarrow \text{vdW} \rightarrow \text{SP} \rightarrow \alpha\text{-TOH}{-}\text{OH}$$

Figure 4 plots the optimized geometries at Level 0. The first stationary point is a van der Waals complex, where the OH radical approaches parallel to the aromatic ring, with a bond distance $O-C_6$ of 2.658 Å. This approach and the relative stability (see later) is favored for the existence of an additional hydrogen bond between the oxygen of the OH radical and the phenolic hydrogen, with a bond distance of 2.129 Å (note that then the van der Waals denomination is only descriptive).

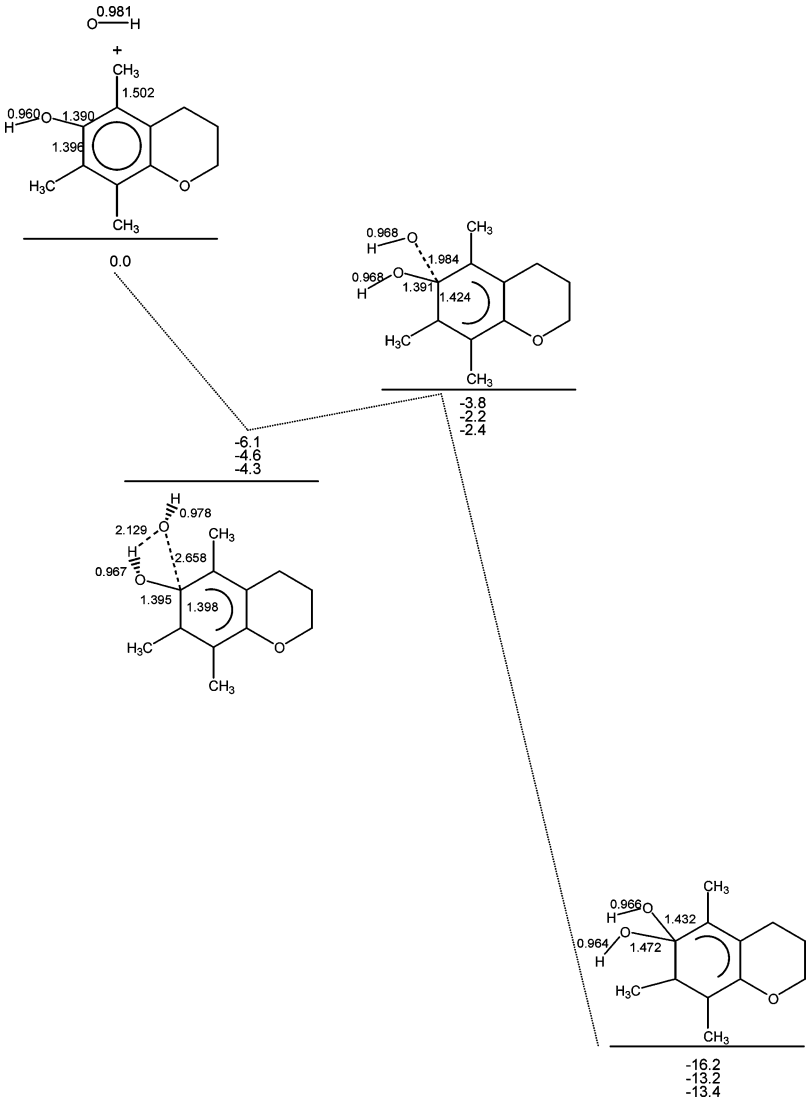

Figure 4. Reaction and barrier height energy (first entry) and enthalpy at 0 K (second entry) and 298 K (third entry) and geometric (bond lengths in angstroms) reaction profile of the OH + α-tocopherol addition reaction, Radd2, computed at the BHandHLYP/6-31G level of theory.

Subsequently, a closer approach of the OH radical led us to a true saddle point. The bond being formed is significantly stretched, being somewhat longer than a single C−O bond (1.435 Å in methanol, for instance).

3.3.1. Relative Energies. The energy and enthalpy changes (0 and 298 K) of reaction and activation (estimated at the saddle point) for the Radd2 reaction at Level 0 are also plotted in Figure 4. Unfortunately, comparison of these magnitudes with experimental or theoretical work is not possible because there have been no measurements in either case. To analyze the influence of the level of calculation, the energy and enthalpy changes at 298 K using different levels are also listed in Table 2. As in the case of the hydrogen abstraction mechanism, the reaction is more exothermic the higher the level of calculation.

With respect to the saddle point, leaving aside Level 1 (MPW1K functional), as the level of calculation increases, the barrier height is higher, although unlike the hydrogen abstraction reaction, all levels give negative values. The van der Waals complex in the entry channel is weakly bound, and like the hydrogen abstraction reaction, its stability decreases as the level of calculation increases and the thermal effects are considered. Thus, at the highest, Level 3 at 298 K, its enthalpy stability is reduced to 1.9 kcal/mol and hence has little influence on the mechanism of the reaction.

TABLE 3: Rate Constants and Transmission Coefficients for the Rabs2 and Radd2 Reactions (M^{-1} s^{-1}) at the Level 3///Level 0 Dual-Level

	Rabs2			Radd2[a]
T (K)	CVT	SCT	CVT/SCT	CVT/SCT
250	2.8(7)[b]	1.76	4.9(7)	2.7(8)
275	3.3(7)	1.62	5.3(7)	2.3(8)
298	3.7(7)	1.52	5.6(7)	2.2(8)
300	3.7(7)	1.51	5.6(7)	2.2(8)
325	4.3(7)	1.43	6.1(7)	2.0(8)
350	4.9(7)	1.36	6.6(7)	1.9(8)
400	6.1(7)	1.27	7.7(7)	1.7(8)

[a] In the addition reaction, CVT/SCT = CVT because the transmission coefficient is unity over the whole temperature range. [b] 2.8(7) stands for 2.8×10^7.

3.4. Kinetics. After calculating the respective saddle points, we followed the reaction paths independently for the two reactions, Rabs2 and Radd2, at Level 0, and used this information to perform a dual-level kinetics calculation, Level 3///Level 0, to obtain the CVT rate constants and SCT transmission coefficients. The resulting CVT/SCT dual-level rate constants are listed in Table 3 for the temperature range 250−400 K. (Note that this range is very broad for a biological system, but it

permits a clearer interpretation of the temperature dependence of the rate constants.) Several features merit discussion.

First, the transmission coefficient, which mostly takes into account quantum effects on the motion along the reaction path, slightly increases the abstraction reaction rate by a factor of 1.52 at 298 K but does not influence the addition reaction.[31] This behavior was to be expected, since the abstraction reaction presents a low barrier (+0.8 kcal/mol at Level 3) and involves the motion of a light particle (a hydrogen atom) that can tunnel through the reaction barrier, while the addition reaction is a barrierless reaction and involves the movement of heavy atoms. Indeed, at 298 K, only 36% of the abstraction reaction is due to tunneling.

Second, the rate constants for the addition reaction are greater than those for the abstraction reaction, by factors of between 5 and 2 over the whole temperature range. For instance, at 298 K, the rate constants are 2.2×10^8 versus 5.6×10^7 M^{-1} s^{-1}, respectively; that is, at room temperature, the abstraction represents about 20% of the overall OH radical reaction, which is the expected behavior of OH electrophilic reactions.[33] While the calculated rate constants for the abstraction reaction show a positive temperature dependence, and consequently a positive activation energy, the corresponding values for the addition reaction show a negative variation, and consequently a negative activation energy. The activation energy can be obtained from the rate constants through the usual definition

$$E_a(T) = R\frac{d(\ln k)}{d(1/T)}$$

with R being the gas constant, which is equivalent to determining the slope of the Arrhenius plot. At 298 K, our best estimates are +0.5 and −0.8 kcal/mol for the Rabs2 abstraction and Radd2 addition reactions, respectively. These results agree qualitatively with those obtained for the CoQ + OH reaction,[4] where the electrophilic OH addition on the oxidized form (ubiquinone) is also the dominant mechanism, although in this case, the theoretical rate constant at 298 K is larger, 2.1×10^{10} M^{-1} s^{-1}, and the activation energy is lower, −4.0 kcal/mol.

Third, as we noted above, in the reaction of α-TOH with the hydroxyl radical, the two mechanisms are competitive, and therefore, the total rate constant will be

$$k(T) = k_{abs}(T) + k_{add}(T)$$

that is, at 298 K, we obtain a total rate constant of 2.7×10^8 M^{-1} s^{-1}. Moreover, taking into account that all eight reactions are very exothermic (Table 1), we can assume that the attack of the OH radical on the other positions, Rabs1, Rabs3, and Rabs4, on one hand, and Radd1, Radd3, and Radd4, on the other, will also contribute to the final rate constant, although obviously to a lesser degree. Therefore, to make comparison possible with future experimental measurements, the earlier value represents only the lower limit of the rate constant for this reaction. We thus propose a final value of k(298 K) ≥ 2.7×10^8 M^{-1} s^{-1}, with an activation energy of −0.5 kcal/mol.

3.5. Comparison with Analogous Biological Systems. This addition mechanism is supported by the experimental evidence in analogous reactions and is a common pathway for other biological systems. Table 4 lists some such systems together with the title reaction at room temperature. All systems present strong scavenging activity with respect to the OH radical, with very high rate constants that are practically diffusion-controlled. The α-TOH and CoQ cases represent the lower and upper limits of the selected group.

TABLE 4: Mechanism and Rate Constants for Several Biological Compounds with OH, at 298 K, in M^{-1} s^{-1}

compound	mechanism	rate constant	reference
α-TOH	addition	2.2(8)	this work
thymine	addition	1.7(9)	34, 35
uracyl	addition	2.6(9)	34
NADH[a]	addition	2.0(10)	36
melatonin	addition	2.7(10)	37, 38
CoQ	addition	6.2(10)	4

[a] Nicotinamide adenine dinucleotide.

TABLE 5: Antioxidant Activity of α-TOH and CoQ with Two Damaging Free Radicals, OH and OOH

antioxidant	radical	mechanism	rate constant	reference
CoQ	OH	addition	6.2(10)	4
	OOH	abstraction	5.3(5)	5
α-TOH	OH	addition	≥2.7(8)	this work
	OOH	abstraction	1.5(5)	6

Finally, Table 5 presents the different behaviors of the two liposoluble natural antioxidants, α-TOH and CoQ, against the OH and OOH radicals, as analyzed by our group in recent years. First, against these two radicals, CoQ has a stronger scavenging activity than α-TOH, which agrees with the experimental evidence in LDL, that is, an apolar environment congruent with the theoretical model analyzed here. Second, the OH free radical gives addition reactions, while the OOH free radical gives abstraction reactions. Thus, OH behaves more as an electrophilic compound than as a free radical, while OOH behaves as a typical free radical.

4. Conclusions

The theoretical study of antioxidant activity is an interesting field of research. As a continuation of our previous studies on CoQ and α-TOH, we here studied the kinetics and dynamics of the reaction of α-tocopherol with the damaging hydroxyl radical as a prototype of antioxidant process.

The OH radical can attack α-tocopherol by different pathways: hydrogen abstraction reactions from the phenolic O−H and methyl groups (four reactions) and electrophilic OH addition on several positions on the aromatic ring (four reactions). We found that the most favorable mechanisms are the hydrogen abstraction reaction from the phenolic hydrogen, with a low barrier height (+0.8 kcal/mol), and the electrophilic OH addition on carbon 6, which is a barrierless reaction. All eight reactions are strongly exothermic, indicating that the OH radical is only slightly or not at all selective, giving competitive reactions.

We found that the reactivity of the OH radical is dominated by the addition mechanism, with a rate constant of 2.2×10^8 M^{-1} s^{-1} at 298 K, as against the rate constant for the hydrogen abstraction reaction of 5.6×10^7 M^{-1} s^{-1} at 298 K. Hence, we proposed a final rate constant of ≥2.7×10^8 M^{-1} s^{-1} at 298 K, of which the hydrogen abstraction reaction represents about 20%. Although this result for α-TOH is smaller than that observed for CoQ, 6.2×10^{10} M^{-1} s^{-1} at 298 K, by 2 orders of magnitude, the high values of both rate constants indicate that the two natural radical trapping antioxidants provide antioxidant protection to the cell.

The two most favorable abstraction and addition reactions proceed through intermediates in the reactant channel with little or no influence on the dynamics of the reactions. However, the abstraction reaction also presents another highly stabilized complex in the product channel, which could hinder the further reactions of the α-tocopheryl radical that can cause the observed pro-oxidant effects of α-tocopherol. This effect, however, will

be less important than in the case of the OOH radical due to the competitive addition mechanism.

Acknowledgment. This work was partially supported by the Junta de Extremadura (Project Nos. 2PR01A002 and 2PR04-A001).

Supporting Information Available: Cartesian coordinates, energies, and vibrational frequencies for the optimized stationary points computed at Level 0. This material is available free of charge via the Internet at http://pubs.acs.org.

References and Notes

(1) (a) Niki, E. *Free Radical Res.* **2000**, *33*, 693. (b) Pryor, W. A. *Free Radical Biol. Med.* **2000**, *28*, 141.

(2) Bowry, V. W.; Stocker, R.; Walling, C. *Proc. Natl. Acad. Sci. U.S.A.* **1993**, *90*, 45.

(3) For a recent review, see: Niki, E.; Nogichu, N. *Acc. Chem. Res.* **2004**, *37*, 45 and references therein.

(4) Espinosa-García, J.; Gutiérrez-Merino, C. *J. Phys. Chem. A* **2003**, *107*, 9712.

(5) Espinosa-García, J. *J. Am. Chem. Soc.* **2004**, *126*, 920.

(6) Navarrete, M.; Rangel, C.; Espinosa-García, J.; Corchado, J. C. *J. Chem. Theory Comput.* **2005**, *1*, 337.

(7) Foti, M.; Ingold, K. U.; Lusztyk, J. *J. Am. Chem. Soc.* **1994**, *116*, 9440.

(8) (a) Lynch, B. J.; Fast, P. L.; Harris, M.; Truhlar, D. G. *J. Phys. Chem. A* **2000**, *104*, 4811. (b) Zhao, Y.; Lynch, B. J.; Truhlar, D. G. *J. Phys. Chem. A* **2004**, *108*, 4786.

(9) Truong, T. N.; Duncan, W. *J. Chem. Phys.* **1994**, *101*, 7403.

(10) Zhang, Q.; Bell, R.; Truong, T. N. *J. Phys. Chem.* **1995**, *99*, 592.

(11) Durant, J. L. *Chem. Phys. Lett.* **1996**, *256*, 595.

(12) Frisch, M. J.; Trucks, G. W.; Schlegel, H. B.; Scuseria, E.; Robb, M. A.; Cheeseman, J. R.; Zakrzewski, V. G.; Montgomery, J. A.; Stratman, R. E.; Burant, J. C.; Dapprich, S.; Millam, J. M.; Daniels, A. D.; Kudin, K. N.; Strain, M. C.; Farkas, O.; Tomasi, J.; Barone, V.; Cossi, M.; Cammi, R.; Menucci, B.; Pomelli, C.; Adamo, C.; Clifford, S.; Ochterki, J.; Petterson, G. A.; Ayala, P. Y.; Cui, Q.; Morokuma, K.; Malik, D. K.; Rabuk, A. D.; Raghavachari, K.; Foresman, J. B.; Cioslowski, J.; Ortiz, J. V.; Stefanov, J. J.; Liu, G.; Liashenko, A.; Piskorz, P.; Komaromi, I.; Gomperts, R.; Martin, R. L.; Fox, D. J.; Keith, T.; Al-Laham, M. A.; Peng, C. Y.; Nanayakkara, A.; González, C.; Challacombe, M.; Gill, P. M. W.; Johnson, B. G.; Chen, W.; Wong, M. W.; Andres, J. L.; Head-Gordon, M.; Reploge, E. S.; Pople, J. A. *GAUSSIAN98*, revision A.7; Gaussian Inc.: Pittsburgh, PA, 1998.

(13) Becke, A. D. *J. Chem. Phys.* **1993**, *98*, 1372−1377.

(14) Lee, C.; Yang, W.; Parr, R. G. *Phys. Rev. B* **1988**, *37*, 785−789.

(15) Hehre, W. J.; Ditchfield, R.; Pople, J. A. *J. Chem. Phys.* **1972**, *56*, 2257−2261.

(16) Hehre, W. J.; Radom, L.; Schleyer, P. v. R.; Pople, J. A. *Ab initio Molecular Orbital Theory*; Wiley: New York, 1987.

(17) Fast, P. L.; Truhlar, D. G. *J. Chem. Phys.* **1998**, *109*, 3721−3729.

(18) Chuang, Y.-Y.; Truhlar, D. G. *J. Phys. Chem. A* **1998**, *102*, 242−247.

(19) See, for example: Truhlar, D. G.; Gordon, M. S. *Science* **1990**, *249*, 491−498 and references therein.

(20) Corchado, J. C.; Coitiño, E. L.; Chuang, Y.-Y.; Fast, P. L.; Truhlar, D. G. *J. Phys. Chem. A* **1998**, *102*, 2424−2438.

(21) For a recent review on these methods, see: Truhlar, D. G.; Gao, J.; García-Viloca, M.; Alhambra, C.; Corchado, J. C.; Sánchez, M. L.; Poulsen T. D. *Int. J. Quantum Chem.* **2004**, *100*, 1136−1152.

(22) Corchado, J. C.; Chuang, Y.-Y.; Fast, P. L.; Villà, J.; Hu, W.-P.; Liu, Y.-P.; Lynch, G. C.; Nguyen, K. A.; Jackels, C. F.; Melissas, V. S.; Lynch, B. J.; Rossi, I.; Coitiño, E. L.; Fernandez-Ramos, A.; Pu, J.; Albu, T. V.; Steckler, R.; Garrett, B. C.; Isaacson, A. D.; Truhlar, D. G. *POLYRATE*, version 9.0; University of Minnesota: Minneapolis, MN, 2002.

(23) Corchado, J. C.; Coitiño, E. L.; Chuang, Y.-Y.; Truhlar, D. G. *GAUSSRATE*, version 9.0; University of Minnesota: Minneapolis, MN, 2002.

(24) Chuang, Y.-Y.; Corchado, J. C.; Truhlar, D. G. *J. Phys. Chem. A* **1999**, *103*, 1140−1149.

(25) Corchado, J. C.; Espinosa-García, J.; Hu, W.-P.; Rossi, I.; Truhlar, D. G. *J. Phys. Chem.* **1995**, *99*, 687−694.

(26) Berkowitz, J.; Ellison, G. B.; Gutman, D. *J. Phys. Chem.* **1994**, *98*, 2744−2765.

(27) Wayner, D. D. M.; Lusztyk, E.; Ingold, K. U.; Mulder, P. *J. Org. Chem.* **1996**, *61*, 6430−6433.

(28) Hammond, G. S. *J. Am. Chem. Soc.* **1955**, *77*, 334.

(29) *JANAF Thermochemical Tables*, 3rd ed.; Chase, M. W., Jr., Davies, C. A., Downey, J. R., Frurip, D. J., McDonald, R. A., Syverud, A. N., Eds.; National Bureau of Standards: Washington, DC, 1985; Vol. 14.

(30) In the original paper (ref 5), the product well was not plotted in Figure 1. In fact, this figure in ref 5 should be completed with a hydrogen bonded complex before products, with a stabilization of −13.4 kcal/mol with respect to the products at Level 0.

(31) Note that the transmission coefficient κ not only is a tunneling correction but also takes into account three effects: tunneling, which tends to make $\kappa > 1$, nonclassical reflection of trajectories that classically would overcome the barrier, which tends to make $\kappa < 1$; and a better treatment of the reaction threshold than the canonical variational transition-state theory, which also makes $\kappa < 1$. The net effect in the abstraction reaction is $\kappa > 1$, while, in the addition reaction, it is $\kappa < 1$. For a detailed description of the calculation of transmission coefficients and threshold corrections, see ref 32.

(32) Truhlar, D. G.; Isaacson, A. D.; Garrett, B. C. In *Theory of Chemical Reaction Dynamics*; Baer, M., Ed.; CRC Press: Boca Raton, FL, 1985; Vol. 4, pp 65−137.

(33) Seinfeld, J. H.; Pandis, S. N. *Atmospheric Chemicstry and Physics*; John Wiley: New York, 1998.

(34) Javanovic, S. V.; Simic, M. G. *J. Am. Chem. Soc.* **1986**, *108*, 5968.

(35) Cadete, J.; Delatour, Th.; Douki, Th.; Gasparutto, D.; Pauget, J.-P.; Ravanat, J.-L.; Sauvaigo, S. *Mutat. Res.* **1999**, *424*, 9.

(36) Goldstein, S.; Czapski, G. *Chem. Res. Toxicol.* **2000**, *13*, 736.

(37) Matuszak, Z.; Reszka, K. J.; Chignell, C. F. *Free Radical Biol. Med.* **1997**, *23*, 367.

(38) Turjanski, A. G.; Rosenstein, R. E.; Estrin, D. A. *J. Med. Chem.* **1998**, *41*, 3684.